

## Research Article

**Cite this article:** Ait Oumeziane A, Parisse J-D (2019). Dynamics of UV short pulse laser-induced plasmas from a ceramic material “titanium carbide”: a hydrodynamical out of equilibrium investigation. *Laser and Particle Beams* **37**, 86–100. <https://doi.org/10.1017/S0263034619000168>

Received: 15 January 2019

Revised: 4 February 2019

Accepted: 15 February 2019

**Key words:**

Inverse Bremsstrahlung; laser-induced plasma; photoionization; plasma dynamics; shock waves excimer lasers; titanium carbide

**Author for correspondence:**

A. Ait Oumeziane, Department of Mechanical Engineering and Energetics, Aix-Marseille University, Marseille, 13013, France.  
E-mail: [amina.aitoumeziane@outlook.fr](mailto:amina.aitoumeziane@outlook.fr)

# Dynamics of UV short pulse laser-induced plasmas from a ceramic material “titanium carbide”: a hydrodynamical out of equilibrium investigation

A. Ait Oumeziane<sup>1–4</sup> and J-D. Parisse<sup>2,5</sup>

<sup>1</sup>Department of Mechanical Engineering and Energetics, Aix-Marseille University, Marseille, 13013, France; <sup>2</sup>IUSTI UMR CNRS 7343, 5 rue Enrico Fermi, 13013, Marseille, France; <sup>3</sup>IMT Mines Albi-Carmaux, Albi, 81000, France; <sup>4</sup>Centre RAPSODEE UMR CNRS 5302, campus Jarlard, route de Teillet, 81000 Albi and <sup>5</sup>French Air Force Academy Salon de Provence, France

**Abstract**

The present work is motivated by the numerous applications of short lasers–ceramics interaction. It aims at applying a newly developed model to investigate the dynamic of laser-induced plasmas from a ceramic material into a helium gas under atmospheric pressure. To have a better understanding of the link between the material properties, the plume characteristics and its interaction with the laser beam, a thorough examination of the entire ablation processes is conducted. Comparison with the behavior of laser-induced plumes under the same conditions from a pure material is shown to have a key role in shedding the light on what monitors the plume expansion in the background environment. Plume temperatures, velocities, ionization rates as well as elemental composition have been presented and compared under carefully chosen relevant conditions. This study is of interest for laser matter applications depending on the induced plasmas dynamics and composition.

**Introduction**

Due to their unique characteristics, plasmas induced from laser ablation are at the core of numerous applications. Thin film coating using pulsed laser deposition (PLD) (Dellasega *et al.*, 2017), spectrochemical analysis by means of laser-induced breakdown spectroscopy (Siozos *et al.*, 2017; Koral *et al.*, 2018), propulsion of space craft using laser ablation thrusters (Yu *et al.*, 2018), as well as inertial fusion confinement (Strozzi *et al.*, 2017), are all based upon the ruling mechanisms behind the formation and expansion of laser-induced plasmas (LIP). Whether for practical applications or for the ones which are still at the experimental stage, fundamental research aiming at understanding how the target nature (thermophysical and optical properties) as well as the laser beam properties and the background environment impact the initial stage of the plasma plume creation and its dynamic remains crucial. Since the laser–target/laser–plasma interactions as well as the dynamic and composition of the laser-induced plume play a key role in the transfer of the target stoichiometry, the deposition rate of thin films and their properties using PLD, numerous works have been dedicated to investigating titanium carbide (TiC) film deposition using short and ultrashort laser pulses, with the majority being experimental (D’Alessio *et al.*, 1998; Kumar *et al.*, 1998; Teghil *et al.*, 2001, 2006; Oliveira *et al.*, 2005). Kumar *et al.* (1998) have worked on the optimization of PLD conditions to obtain thin films with the best crystalline quality structure and mechanical properties. They found out that thin films deposited at relatively high temperatures are more mechanically resistant. Teghil *et al.* (2006) used a femtosecond laser pulsed to deposit nanostructured TiC thin films on silicon wafers. The results of their experiments revealed that the thin films are mainly constituted of melted nanoparticles directly ejected from the target and crystals produced by gas phase condensation. In another work, Teghil *et al.* (2001) studied TiC and TaC thin film deposition on silicon substrate using a 532 nm, 10 ns Nd:YAG laser pulse with a 10 Hz repetition rate. They managed to link the laser-induced plumes characteristics to each target properties and the modality of the thin films growth to each ablation process. D’Alessio *et al.* (1998) defined an optimal evaporation regime as a function of the laser fluence for depositing high-quality TiC thin films on a glass plate substrate. The target stoichiometry was also successfully preserved. This work, where a 532 nm, 10 ns Nd:YAG laser pulse with a 10 Hz repetition rate was also used, revealed a link between the films directionality and the plumes. Oliveira *et al.*’s (2005) work aimed at defining the mechanisms behind an undesirable phenomenon during laser processing of TiC and TiC composites which is column-growth. A laser fluence range has been suggested to avoid the shadowing mechanism which has been shown to be at the origin of the column formation. A few modeling approaches

aiming at examining TiC laser ablation processes for PLD parameters optimization (Oliveira and Vilar, 2007; Vasantgadkar *et al.*, 2010) are present in the literature. Oliveira and Vilar (2007) suggested a 2D finite element model to simulate laser ablation of a TiC target. The laser material interaction was described using a thermal model and the role of the LIP was considered through an optical thickness coefficient estimated partly through experimental data. The likelihood of the role played by the explosive boiling mechanism in the ablation process under the considered laser fluences was discussed and the importance of avoiding it for high-quality thin film deposition was emphasized. Vasantgadkar *et al.* (2010) adopted relatively the same model as Oliveira and Vilar (2007). They mainly focused on the impact of considering the temperature dependency of the material optical properties on improving the prediction of the ablation depths and the increase of their agreement with experimental data. The particularity of our approach is that we describe the ablation process as a whole through a thermal model for the pulse–target interaction coupled with an out of equilibrium model for the plasma formation and expansion. In a previous work (Ait Oumeziane *et al.*, 2016a), we investigated the ablation process under the same conditions of two metals namely titanium and copper. A comparison between target melting and evaporation thresholds was presented along with ablation depths and plasma ignition thresholds. Results for both materials differ considerably. Those discrepancies have been linked to the targets properties especially their thermal conductivity which has been shown to be the one governing the ablation process. More recently we have developed a new model to describe the ablation process of a multicomponent target (Ait Oumeziane and Parisse, 2018). The latter has been applied to TiC with a focus on comparing processes in the material such as melting and ablation depths and thresholds as well as plasma shielding rates induced under the same conditions from a pure titanium material. Plume electronic and heavy species temperatures and densities have also been presented and the thermal no equilibrium investigated. However, in this preliminary study the plasma dynamic has not been the center of interest. The present paper is dedicated to investigating the dynamic of LIP from a ceramic material. To have a better understanding of the link between the material properties and the plume characteristics and dynamic, a thorough examination of the entire ablation processes is made. Results comparison with the behavior of laser-induced plumes under the same conditions from a pure material is shown to have a key role in shedding the light on what monitors the plume expansion in the background environment. Plume temperatures, velocities, ionization rates as well as elemental composition have been presented and compared under carefully chosen relevant conditions which will be defined later.

## The model

In the following section, we give a detailed description of the physics upon which our model is based.

### Laser–material interaction

For a metallic ceramic material, characterized by a metallic electronic structure such as TiC (Williams, 1999), free electrons present in the conduction band are the ones responsible for the laser beam photons energy absorption and its transfer to the lattice. In the case of nanosecond laser pulses interaction with metallic ceramic materials, thermal equilibrium between the electrons

and the lattice can be assumed. This is due to the electrons–phonon relaxation  $\tau_{e-ph}$  time which varies between  $10^{-12}$  and  $10^{-10}$  s in the case of metallic materials (Williams, 1999). Hence thermalization between the electrons and the lattice occurs at a fraction of the total pulse duration. For that reason, nanosecond laser pulses interaction with TiC can be described through a one temperature thermal model (Ait Oumeziane and Parisse, 2018). At the course of our research development (Ait Oumeziane *et al.*, 2014, 2016a, 2016b; Ait Oumeziane and Parisse, 2018) we have always chosen to adopt an enthalpic formulation of the heat equation [Eq. (1)], which greatly facilitates the phase changes (solid/liquid, liquid/vapor) management. In addition, thermophysical and optical properties were always assumed only phase-dependent (Table 1).

$$\frac{\partial H}{\partial t} = \frac{\partial(\kappa(\partial T/\partial x))}{\partial x} + S_q \quad (1)$$

$$S_q = \alpha_0 I(x, t) \quad (2)$$

$H$ ,  $T$ ,  $\lambda$ ,  $\alpha_0$  are the enthalpy, the temperature, the thermal conductivity, and the absorption coefficient of the material.  $I(x, t)$  is the laser intensity transmitted at the  $x$  depth inside the material and at the “ $t$ ” time. The evolution  $I(x, t)$  is given by the Beer–Lambert law (Van Driel, 1986):

$$I(x, t) = (1 - R)I_0(t)e^{-\alpha_0 x} \quad (3)$$

where  $R$  is the reflectivity of the irradiated surface and  $I_0(t)$  is the incident laser intensity.

A one-dimensional (1D) description of the laser beam interaction with the target material is suitable because the thermal diffusion length of TiC under the present conditions is largely greater than the laser beam penetration depth. In addition, the standard excimer beam radii and the assumed material thickness enable us to neglect the lateral diffusion heat flux and consider the space-time computational domain large enough to assume its outer boundary unaffected by the laser pulse absorption and heat diffusion (Ait Oumeziane *et al.*, 2016a). At the target surface, a zero-heat flux boundary condition is assumed up to the time the surface starts to evaporate.

### Hydrodynamical phenomena

When the laser pulse energy exceeds the material evaporation threshold, the material in the liquid phase undergoes a phase change and a vapor is formed above the target surface. The laser beam is then absorbed partly by the vapor before reaching the still liquid surface of the material. This absorption results in the formation of excited and ionized species which constitute a LIP. The plasma absorbs a certain amount of the laser beam energy and expands toward it. The fact that the plasma absorbs a part of the laser beam is called plasma shielding because it reduces the amount of the laser beam that reaches the material surface. During its expansion, the plasma compresses the background gas, which is helium in the present study. The difference between the pressure in the LIP and the background environment is at the origin of the generation of an intense shock wave. Depending on the target material and the characteristics of the thin film that needs to be deposited, PLD can either be realized in a reactive or a non-reactive atmosphere (Stafe *et al.*, 2014).

**Table 1.** TiC and Ti thermophysical and optical properties considered in the present study

	Solid state		Liquid state	
	Ti	TiC	Ti	TiC
Specific heat, $C_p$ (J/g/K)	0.52	0.55	0.74	0.93
Mass density, $\rho$ (g/cm <sup>3</sup> )	4.5	4.91	4.11	4.91
$\kappa$ (W/m/K)	0.22	0.23	0.33	0.43
$\Delta h$ (J/g)	365	1000	8893	10 000
Temperatures (K)	1933	3340	3560	5080
Reflectivity, $R$	0.37	0.57	0.37	0.6
Absorption coefficient $\alpha$ (/cm)	$9.22 \cdot 10^5$	$1.8 \cdot 10^6$	$9.22 \cdot 10^5$	$5.5 \cdot 10^5$

The choice of the ambient gas is one of the key parameters to monitor the morphology and the properties of the pulsed laser deposited thin films which are particularly linked to the deposition rate (Eason, 2007). For that purpose, several studies have been conducted to demonstrate the impact of the nature as well as the pressure of the ambient gas on the ablation process and the plume expansion (Sturm *et al.*, 2000; Scharf and Krest, 2002; Mendes and Vilar, 2003; Harilal *et al.*, 2006). Using helium as the background gas for laser deposition of thin films has been shown to be of particular interest. When comparing, for example, Ag thin film deposition under several inert gases, a 0.4 mbar helium background gas has been shown to reduce the plume particles kinetic energy which leads to a maximum thin film deposition rate (Scharf and Krest, 2002). In our previous studies (Ait Oumeziane *et al.*, 2016a; Ait Oumeziane *et al.*, 2014; Ait Oumeziane *et al.*, 2016b), results of nanosecond laser-induced metal plasma ignition threshold in a very low-pressure (10 Pa) helium environment have been shown to be in good agreement with experiments conducted under vacuum (Clarke *et al.*, 1999). For all that which has been said helium is chosen to be the background environment in the present study. The hydrodynamical model used to describe the vapor formation and plasma evolution into a helium background environment (Ait Oumeziane and Parisse, 2018) is based on several hypotheses: the exclusive formation of electrons in the vapor and the 1D unsteady inviscid compressible character of the flow. Each constituent is considered to follow the ideal gas law and the entire mixture is supposed to be quasi-neutral. Consequently, no internal electrical field is considered. Since only a short-term evolution of the plume is investigated, a 1D description is adequate. The plasma extent along the  $x$ -direction during this time range is very small compared to the laser beam radius, which usually varies between 0.05 and 2 mm (Ravindra, 2005).

The model which consists of 1D multi-species Euler equations with mass and energy source terms (Lee, 1985) considers the presence of eight species in the plume. The subscript  $i$  varies from 1 to 8 and designates the species  $i$  as follows (1: Ti, 2: He, 3: Ti\*, 4: Ti<sup>+</sup>, 5: C, 6: C\*, 7: C<sup>+</sup>, and 8: e<sup>-</sup>). The two excited species are intermediate states required for the plasma initiation (Table 2).

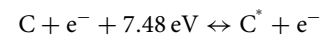
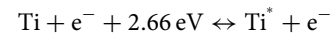
In the present study, a UV 20 ns KrF (248 nm,  $h\nu = 5$  eV) laser pulse, with an ideal Gaussian temporal profile is considered.

The processes governing the dynamic and evolution of the LIP are derived from the kinetic model developed by Rosen *et al.* (1982), they consist of:

**Table 2.** Summary of titanium and carbon atomic state levels considered in the modeling approach used for the present investigation

	Species	Excited state (eV)	Ionization energy (eV)
TiC model	Ti	2.66	6.82
	C	7.48	11.26
Ti model	Ti	2.66	11.26

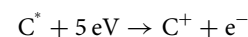
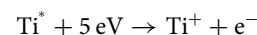
1. The excitations/de-excitation by electronic impact:



2. The ionization/ three body recombination of the excited states by electronic impact:



3. The photoionization of the excited states:



4. The inverse Bremsstrahlung absorption: which considers the electron-neutral (Zel'dovitch and Raizer, 1966) and electron-ion absorptions (Thomann *et al.*, 1997). Hence, the plasma mixture total inverse bremsstrahlung coefficient is the sum of the contribution of the four species (Ait Oumeziane and Parisse, 2018):

$$\alpha_{\text{IB}} = \alpha_{e-i}[\text{Ti}^+] + \alpha_{e-i}[\text{C}^+] + \alpha_{e-n}[\text{Ti}] + \alpha_{e-n}[\text{C}] \quad (4)$$

The kinetic constants of the processes are calculated using a Zel'dovitch's approach (Zel'dovitch and Raizer, 1966) and are used to define the source terms of the hydrodynamical model (Ait Oumeziane and Parisse, 2018):

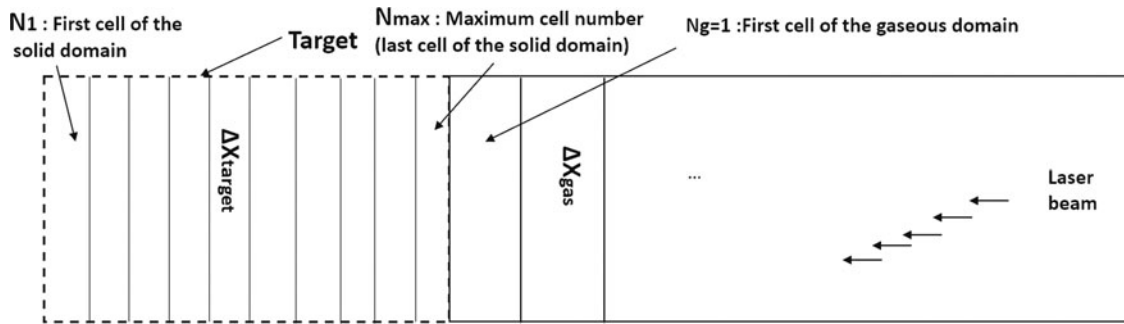


Fig. 1. Solid and gaseous domain grids.

**Boundary conditions and numerical resolution**

The space-time history simulated in this study is extensive enough to assume that the outer boundary of the simulated space-time is not significantly affected by the end of the laser pulse. Thus, the boundary conditions at the origin of the simulated history are simply the initial conditions, which are given by:

$$T(x_{end}) = T_0 = T(t = 0) = 300 \text{ K} \tag{5}$$

For the surface which receives the laser flux, the boundary condition used is a zero flux one for the three equations in solid or liquid phase, because there are no particle or energy fluxes until the boiling begins.

$$\left(\frac{\partial T}{\partial x}\right)_{x=0} = 0. \tag{6}$$

The coupling of the thermal and hydrodynamical solvers allows to have a general and accurate overview of the entire ablation process. Because this code has already been used effectively to simulate laser ablation of semiconductors (Pariße *et al.*, 2011) and metals (Ait Oumeziane *et al.*, 2014, 2016a, 2016b) we know that it is adapted to such multiphysics problems.

In the mathematical formulation of our model  $x = 0$  designates the target surface.  $x_{end}$  on the other hand is chosen so the boundary condition  $T(x_{end}) = 300 \text{ K}$  (which expresses a semi-infinite slab hypothesis) can be valid. After calculating the thermal diffusion length and laser beam penetration width,  $x_{end}$  is set to be largely greater than both. Hence the validity of the semi-infinite slab hypothesis and the boundary condition that expresses it is insured. Numerically  $x = 0$  corresponds to the maximum cell number and  $x_{end}$  the first cell number (Fig. 1) so we can easily estimate the ablation depth by the number of evaporated cells.

In order to solve the thermal model, we chose an explicit central difference scheme, with second-order precision in space and first-order precision in time (Sturm *et al.*, 2000). The time step used for the calculation  $\Delta t$  is equal to  $10^{-15} \text{ s}$ , and the space step is  $\Delta x$  is equal to  $10^{-7} \text{ cm}$ . The hydrodynamic part of our modeling approach is solved using the LCPFCT (Laboratory of Computational Physics Flux Corrected Transport) algorithm (Oran and Boris, 1987; Boris *et al.*, 1993). This explicit algorithm is based upon a finite difference scheme associated with general methods for flux corrected transport. This algorithm is a predictor corrector numerical scheme accurate at the fourth order in space and second order in time (Sturm *et al.*, 2000). A uniform

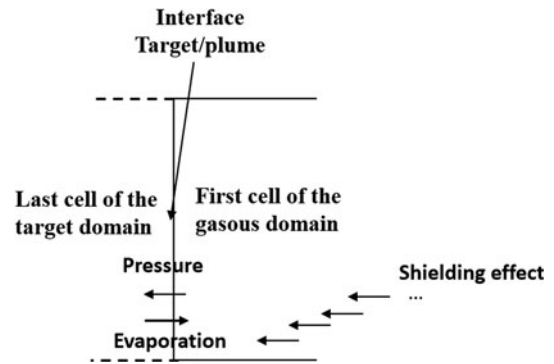


Fig. 2. Target/plume coupling mechanisms.

mesh is used with a space step  $\Delta x$  equal to  $10^{-4} \text{ cm}$  and a time space  $\Delta t$  equal to  $10^{-15} \text{ s}$  as well. The same time step has been used to solve the thermal and hydrodynamic parts of our model, in order to avoid any coupling problem.

**Thermal and hydrodynamical model coupling**

The coupling of the target and the plume is insured through the boiling temperature, the plasma shielding effect, and the mass flow of the vaporized material (Fig. 2).

$$\dot{m} = \rho_{liq} \frac{\Delta x}{\Delta t_{evap}}$$

with:  $\Delta t_{evap}$ : the time for one cell to evaporate  $\Delta x$  the size of the evaporated cell and  $\rho_{liq}$  the liquid mass density where  $(\Delta x / \Delta t_{evap})$  is the variation over time of the thermal ablation depth.

The boiling temperature depends on the pressure of the plume at the material surface. This dependency is expressed by the Clausius–Clapeyron equation:

$$T_{eb} = \frac{1}{((1/T_0) - R(\ln(P_s/P_0)/\Delta H))} \tag{7}$$

$T_0$ : is the boiling temperature,  $P_0$ : the atmospheric pressure,  $P_s$ : the plume pressure,

$\Delta H$ : the latent heat of vaporization and  $R$  the ideal gas constant.

The amount of energy that can reach the target surface depends on how much of the laser beam is absorbed by the plume by inverse Bremsstrahlung as well as photoionization.

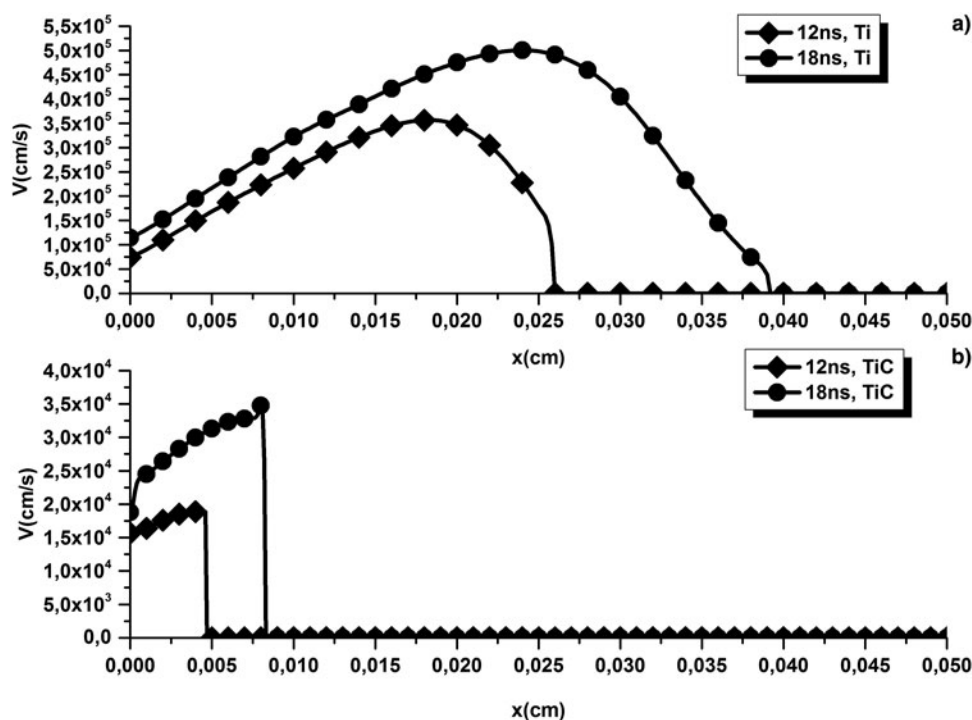


Fig. 3. TiC (b) and Ti (a) plumes velocities for a laser beam fluence of  $15.5 \text{ J/cm}^2$  at 12 and 18 ns.

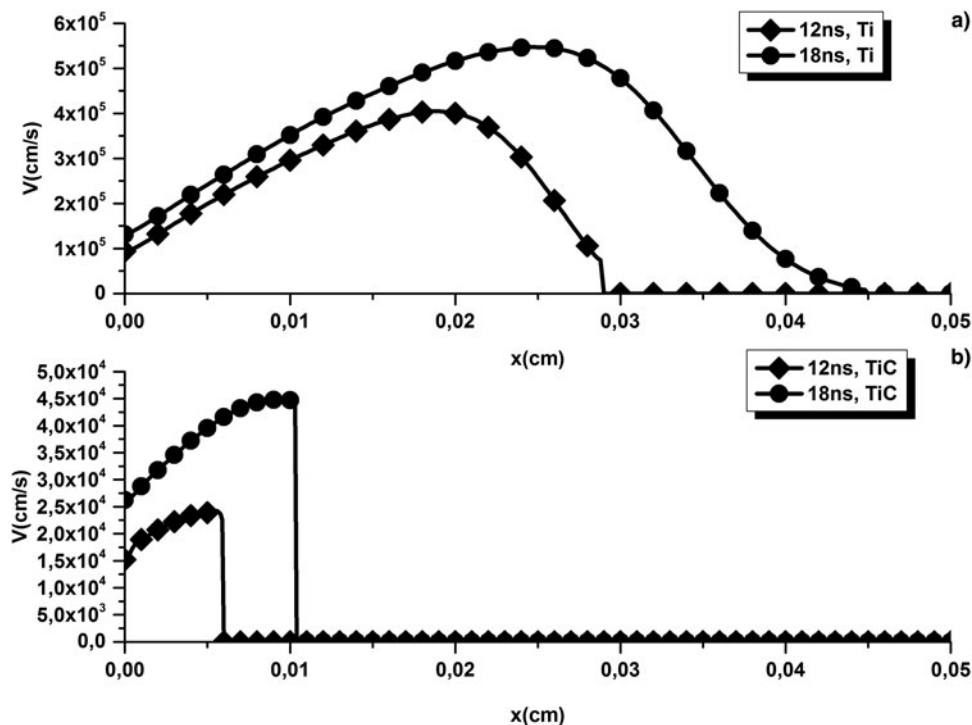
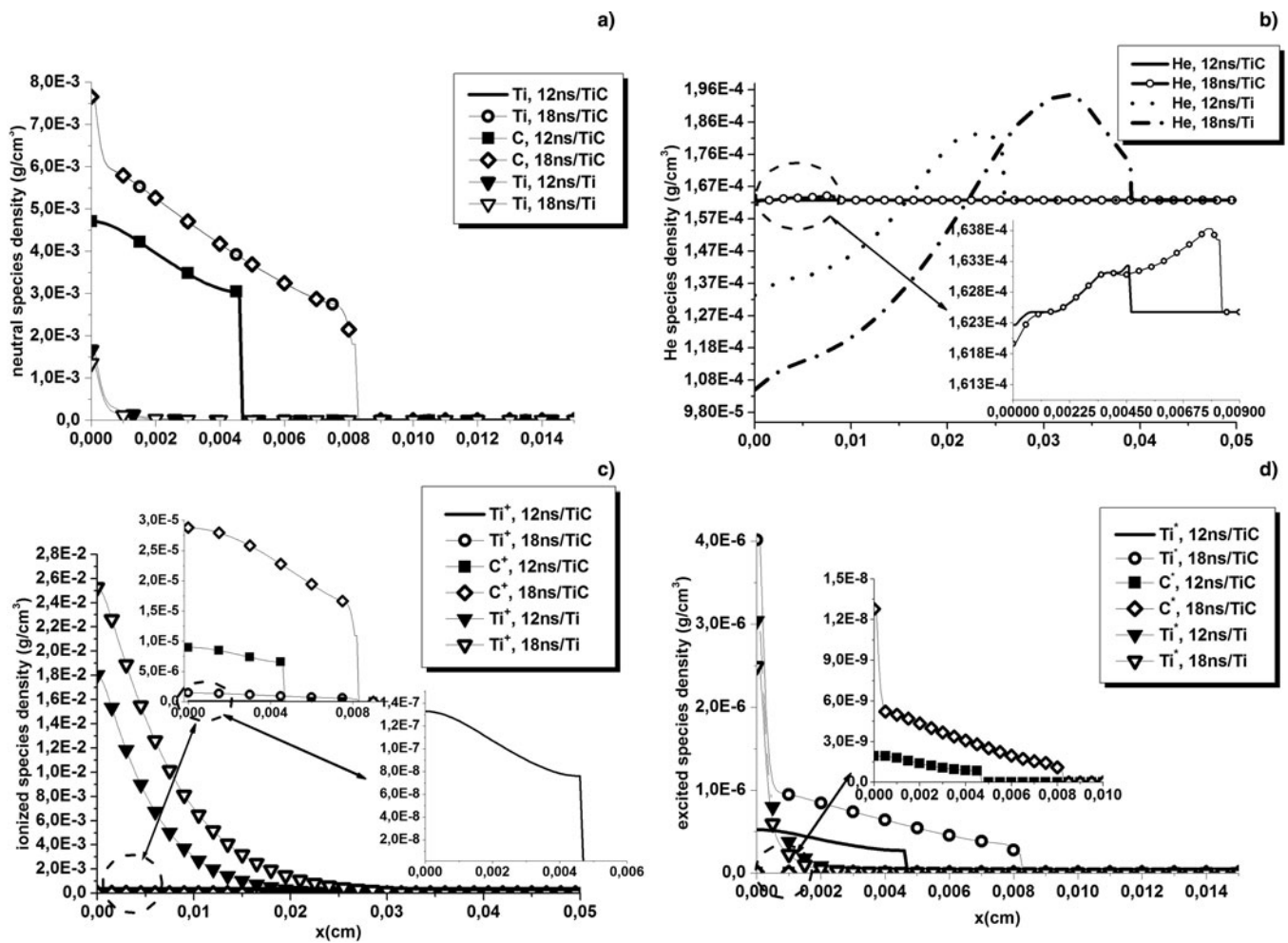


Fig. 4. TiC (b) and Ti (a) plumes velocities for a laser beam fluence of  $20 \text{ J/cm}^2$  at 12 and 18 ns.

Before the start of the evaporation process, the adiabatic condition  $(\partial T/\partial x)_{x=0} = 0$  is used at the interface between the target and the background environment. Once the evaporated matter leaves the surface material, the mass flow  $\dot{m}$  of the vaporized material is calculated, and a total mass, momentum, and energy

balance is done at the first cell of the gaseous domain. The behavior of the evaporated matter is modeled afterwards by the Euler equations.

At the early stage of the material evaporation, the vapor is assumed to be at thermal equilibrium (Mazhukin *et al.*, 2003),



**Fig. 5.** TiC and Ti plumes neutral (a), ionized (c), and excited (d) species mass densities along with He mass density (b) at 12 and 18 ns for a laser beam fluence of 15.5 J/cm<sup>2</sup>.

therefore Boltzmann and Saha’s equations are used to evaluate the densities of the species present in the vapor including the primary electrons.

**Results analysis and discussion**

We remind that for the purpose of the present investigation, a KrF 248 nm, 20 ns full width at half maximum ideal Gaussian laser beam temporal profile has been considered and the ablation process occurs in a helium background environment.

In our previous investigation (Ait Oumeziane and Parisse, 2018), results on processes occurring inside the material, such as phase change thresholds along with ablation depths, have been presented and discussed. Plasma ignition threshold, thermal non-equilibrium as well as species densities have also been focused on. In the present study, we take a step further by focusing on the characterization of the plume dynamics and its connection to the material thermophysical and optical properties. In that purpose the present section will be sequenced as follows:

- Characteristics of TiC laser-induced plumes will be examined and compared with titanium plumes induced under the same conditions. Two laser beam fluences are considered, one below and one above the plasma ignition threshold (Ait

- Oumeziane and Parisse, 2018): 15.5 and 20 J/cm<sup>2</sup>. Although essential, this first step needs to be complemented with other relevant comparison conditions defined in the following point.
- TiC and titanium plumes dynamics and characteristics will be compared for the same effective energy (Ait Oumeziane and Parisse, 2018), the same ablated mass and the same plasma shielding rate.

For all considered cases, the results are presented at two different times, before and after the laser pulse reaches its maximum intensity: 12 and 18 ns.

For the same laser beam fluences: 15.5 J/cm<sup>2</sup> (Fig. 3) and 20 J/cm<sup>2</sup> (Fig. 4), one can see that TiC plumes expansion in the background environment is not as fast as the pure titanium ones. More specifically, at  $t = 12$  ns; the TiC laser-induced plume attains an expansion velocity of  $2 \cdot 10^4$  cm/s for a laser beam fluence of 15.5 J/cm<sup>2</sup> whereas it was able to reach  $3.5 \cdot 10^5$  cm/s in the case of pure titanium. For a laser beam fluence of 20 J/cm<sup>2</sup>, the pure titanium expands until  $3.5 \cdot 10^5$  cm/s whereas the TiC plume reaches  $2.5 \cdot 10^4$  cm/s at best. At  $t = 18$  ns the TiC plume expands 16 times faster than the TiC for a laser beam fluence of 15.5 J/cm<sup>2</sup> and 12 times faster for a laser beam fluence of 20 J/cm<sup>2</sup>. On the other hand, the TiC plumes start their expansion faster than those induced from a pure titanium material but have the

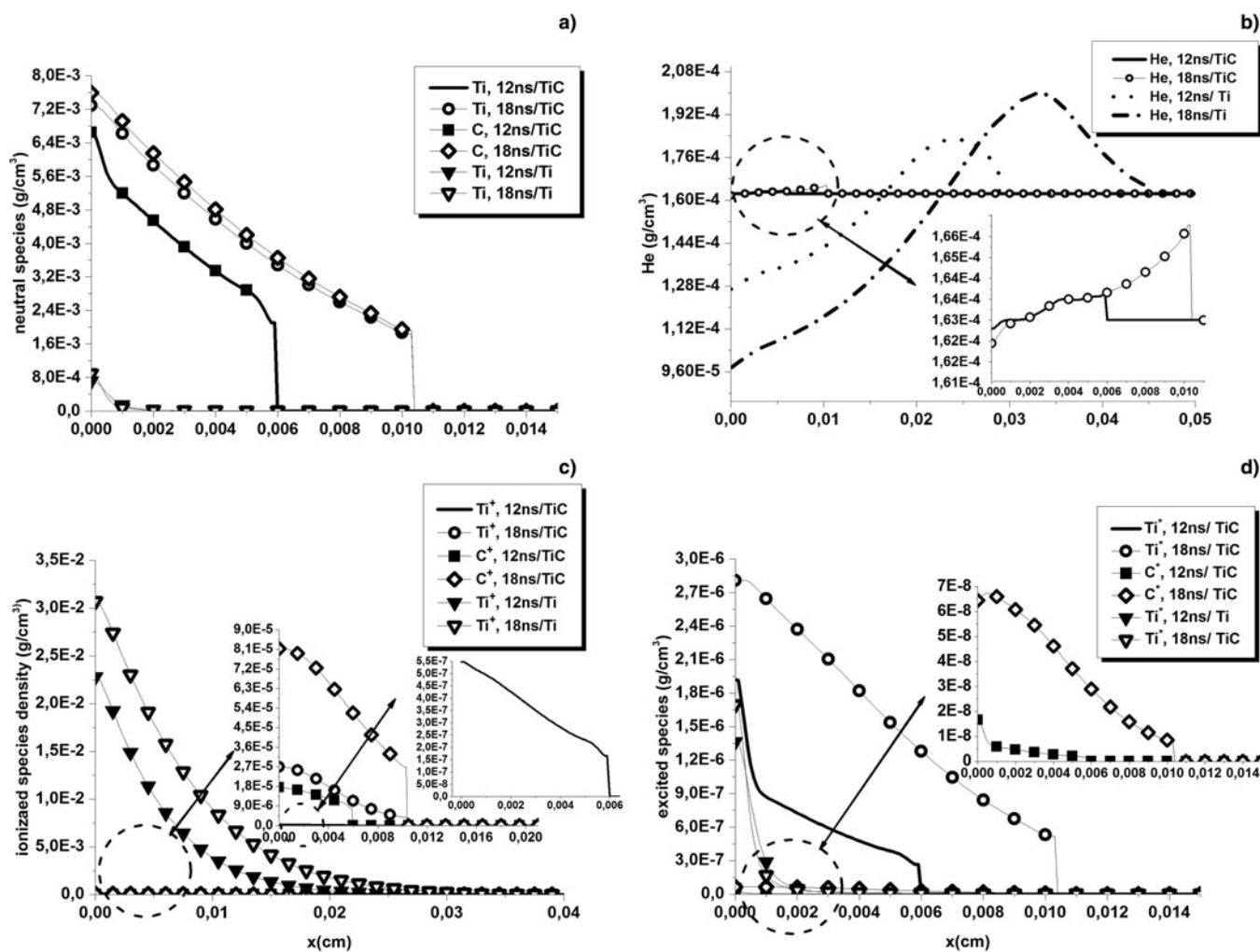


Fig. 6. TiC and Ti plumes neutral (a), ionized (c), and excited (d) species mass densities along with He mass density (b) at 12 and 18 ns for a laser beam fluence of 20 J/cm<sup>2</sup>.

tendency to remain relatively close to the target surface. It is worth noting that for a laser beam fluence of 15.5 J/cm<sup>2</sup> the Ti plume has been induced from a total ablated mass of 4.058·10<sup>-6</sup> g against 1.11·10<sup>-6</sup> g for the TiC plume. On the other hand, for a laser beam fluence of 20 J/cm<sup>2</sup> the Ti plume has been induced from a total ablated mass of 4.95·10<sup>-6</sup> g against 1.12·10<sup>-6</sup> g for the TiC plume. The shielding rates were 69.62 and 71.21% for Ti against 1.07 and 22.5% for TiC for the same laser beam fluences, respectively.

Thermal and optical properties of each target material can partially explain the above-mentioned discrepancies. Aside from the highly reflective character of TiC (its reflectivity is around two times higher than Ti) particularly in the liquid phase, its thermal conductivity as well as its phase transition enthalpies (especially in the solid phase where it is almost three times higher), are the reasons why the TiC laser ablation process needs considerably more input energy and occurs very late in time.

Although the material properties are the origin of the plume formation they are not responsible for its evolution, therefore we need to have a closer look at the plume composition.

Figures 5b and 6b show the classical impact on the plume expansion on the background gas. This complements the velocity results by demonstrating how by its expansion, the TiC plumes

push the background gas away from the target material, increasing its density, but not as much and as far as in the case of the Ti plumes. The decreasing phase of the velocity translates the helium expansion and acceleration behind the resulting shock wave. The time evolution of the shock front position can be followed using either the plume velocity or the background gas density (for which it is more evident) spatial variation at different instants.

Subfigures (a), (c), and (d) of both Figures 5 and 6 show clearly that when it comes to TiC plumes, neutrals are the most dominant species. On the other hand, pure titanium laser-induced plumes are mostly composed of ionized species. This suggests that the plume dynamic may be linked to the nature of the species present in it, especially the dominant ones. Ionized carbon atoms densities are far more important than ionized titanium atoms. This is due to the photoionization process which is more efficient on carbon species because of the smaller gap between its intermediate excited state and its first ionization potential. Carbon atoms have also a higher ionization potential. Therefore, TiC plumes contain more excited titanium species than carbon ones. All species densities increase at  $t = 18$  ns because of the increase of the amount of ablated matter and the efficiency of the inverse Bremsstrahlung and the collisional processes consequently.

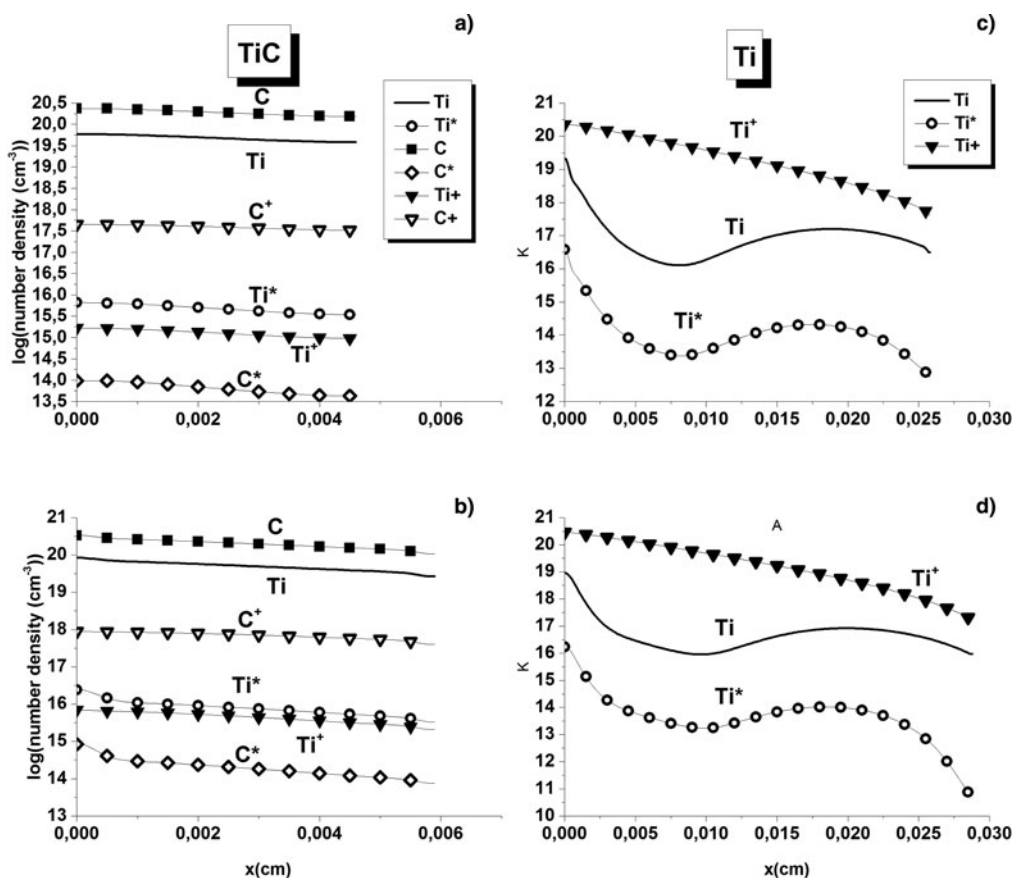


Fig. 7. TiC and Ti plume species number densities logarithm comparison for a laser fluence of 15.5 J/cm<sup>2</sup> (a–c) and 20 J/cm<sup>2</sup> (b–d), respectively, at 12 ns.

Table 3. Conditions for Ti and TiC same ablated mass and effective energy

Material	Laser fluence (J/cm <sup>2</sup> )	Effective energy (J/cm <sup>2</sup> )	Ablated mass (g)
Ti	17	<b>4.84</b>	1.20·10 <sup>-6</sup>
TiC	5	<b>4.70</b>	3.25·10 <sup>-6</sup>
Ti	3	0.75	<b>8.38·10<sup>-7</sup></b>
TiC	12	6.59	<b>8.57·10<sup>-6</sup></b>

Bold values are emphasize when either the effective energy or the ablated mass are approximately equal for Ti and TiC.

Although the plasmas constituents mass densities gave us very useful information for our investigation regarding the plumes dynamics, we thought that looking at the species real amount could reveal even more interesting details. Figures 7 and 8 confirm that the most dominant species in the TiC plumes are indeed neutrals but also show that carbon atoms are the predominant ones. The presence of more ionized carbon species is due to the fact that only 3.78 eV is required to ionize carbon intermediate excited states against 4.16 eV for titanium. At identical times pure titanium plumes contain more ionized titanium than either ionized carbon or ionized titanium present in the TiC plasmas.

Examining each plasma ionization degree (Fig. 9a, b), we found out that the fastest and further away expanding plumes are the ones with the highest ionization degrees, namely, pure titanium laser-induced plumes.

For a thorough investigation of TiC and Ti plasma expansion dynamics and its relation to the nature of species it contains, its ionization degree, we looked for other relevant comparison conditions in our previous investigation (Ait Oumeziane and Parisse, 2018). They are all summarized in Table 3 and consist of interaction conditions for which both targets receive the same effective energy and when the same amount of matter is ablated from each material.

When the plasma is formed above the material surface it partially absorbs the laser beam energy due to the inverse bremsstrahlung and photoionization processes which is known as plasma shielding. The amount of the laser beam that manages to reach the target is what we defined in a previous paper (Ait Oumeziane and Parisse, 2018) as the effective energy.

The results show that four times more laser fluence is required to ablate the same amount of TiC matter as Ti. On the other hand, when both targets receive the same effective energy, more matter is ablated from Ti. This is due to what we discussed earlier regarding each material thermal and optical properties.

When an identical mass is ablated from each target, examining the velocity of the plasma that is formed from it is very interesting (Fig. 10). One can see that in that case and starting from the target surface, titanium plumes also expand faster and further away from the target material. Figure 11 shows the exact same behavior.

Looking back at our previous work (Ait Oumeziane and Parisse, 2018), especially at the plasma shielding, we noted that when identical masses are ablated from each material, TiC plasmas receive <0.5% of the laser beam total energy and <0.005% when the same effective energy reaches each material.



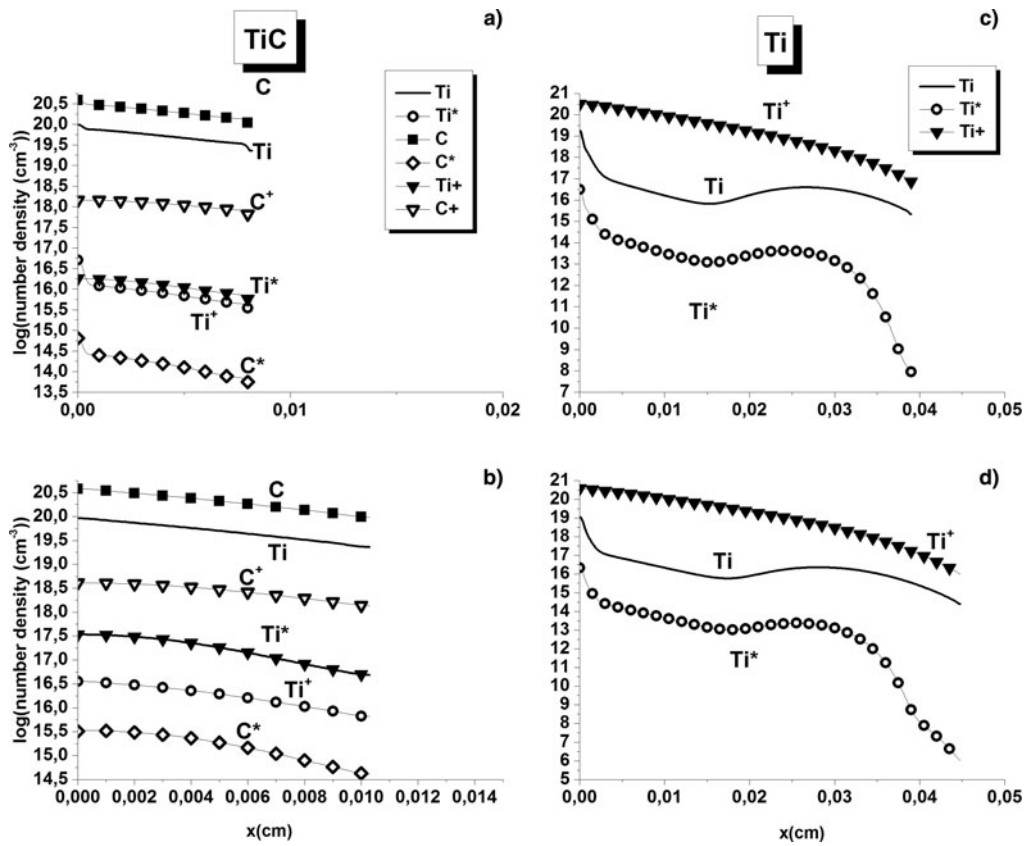


Fig. 8. TiC and Ti plume species number densities logarithm comparison for a laser fluence of 15.5 J/cm<sup>2</sup> (a-c) and 20 J/cm<sup>2</sup> (b-d), respectively, at 18 ns.

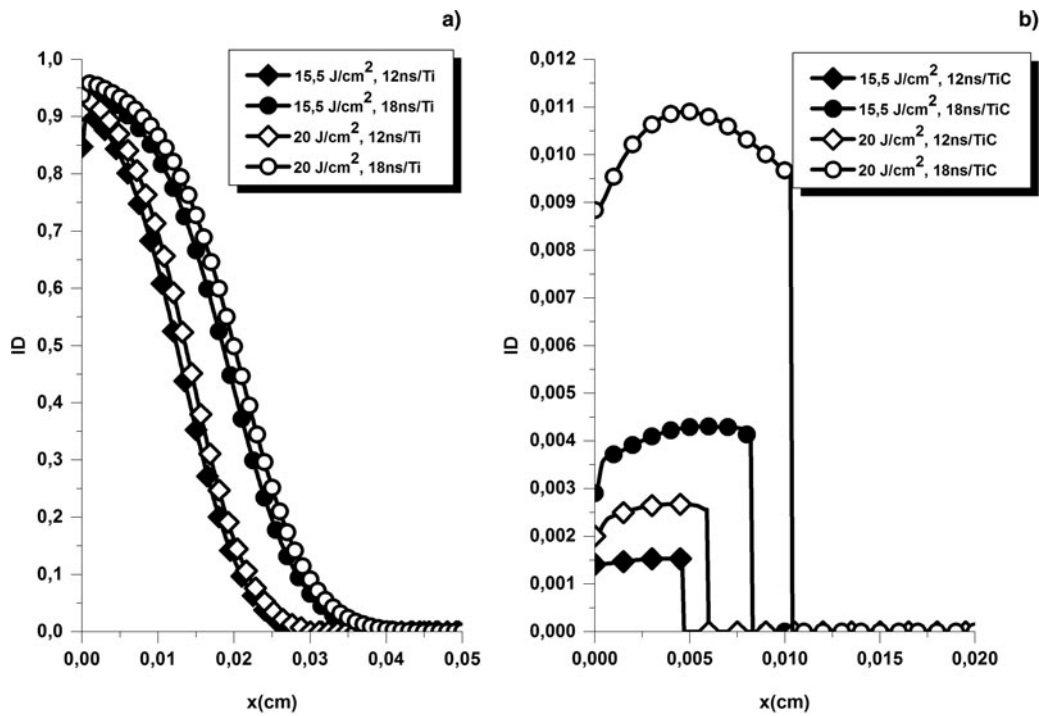


Fig. 9. Ti (a) and TiC (b) plumes ionization degrees for 15.5 and 20 J/cm<sup>2</sup> at 12 and 18 ns.

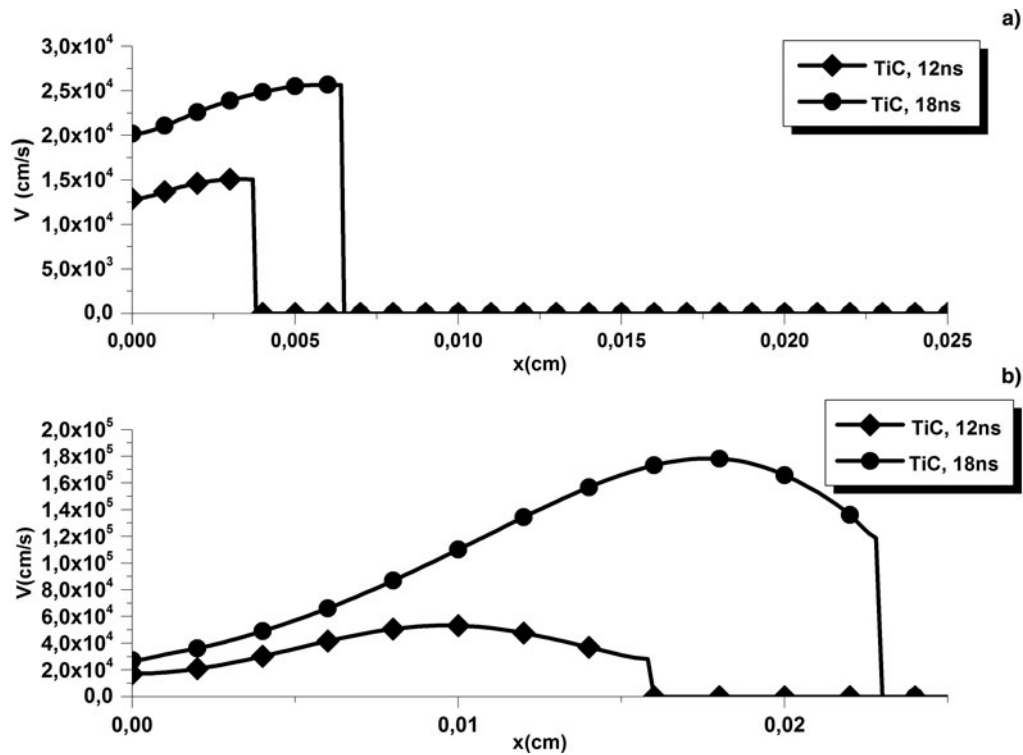


Fig. 10. TiC and Ti plume velocity for the same ablated mass.

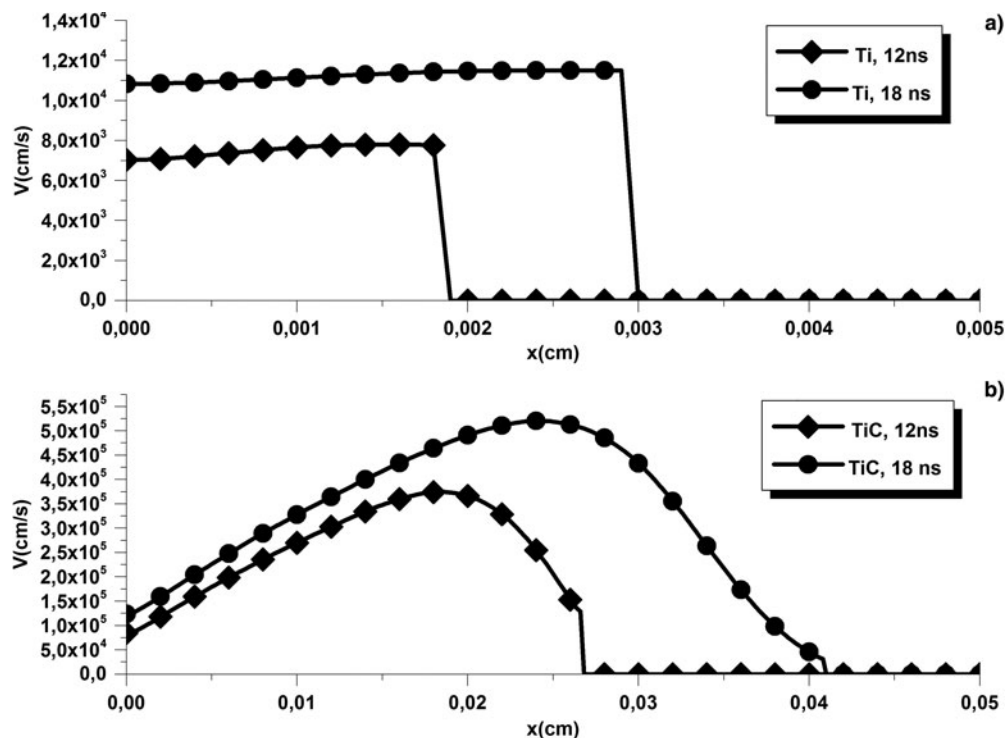


Fig. 11. TiC and Ti plume velocity for the same effective energy.

Either in the case TiC and Ti plumes induced from the same amount of matter (Fig. 12) or when both targets receive the same amount of effective energy (Fig. 13), the results suggest that plumes with neutral species dominance tend to stay relatively confined near the target material. Unlike the same laser beam

fluences cases, in this case and at identical times pure titanium plumes contain less ionized titanium than either ionized carbon or ionized titanium present in the TiC plasmas.

Figures 14 and 15 suggest that either in the plasmas generated from the same of amount matter from TiC and Ti targets or when

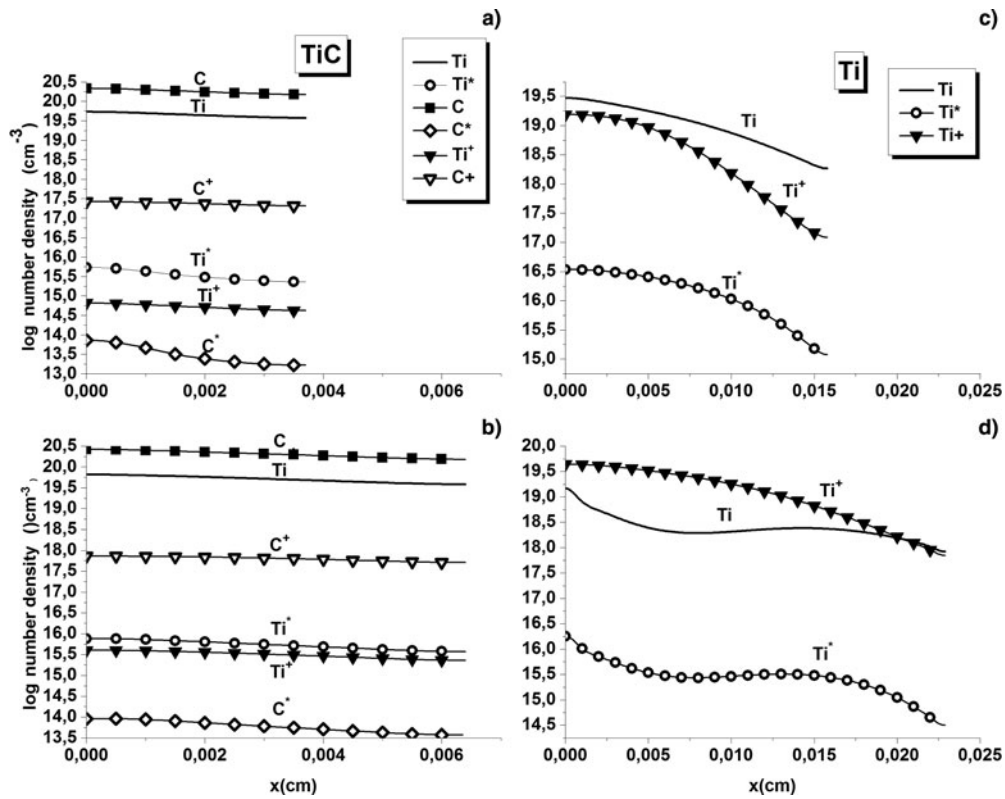


Fig. 12. TiC (a) 12 ns – (c) 18 ns and Ti (b) 12 ns – (d) 18 ns plume species number densities logarithm comparison for the same ablated mass.

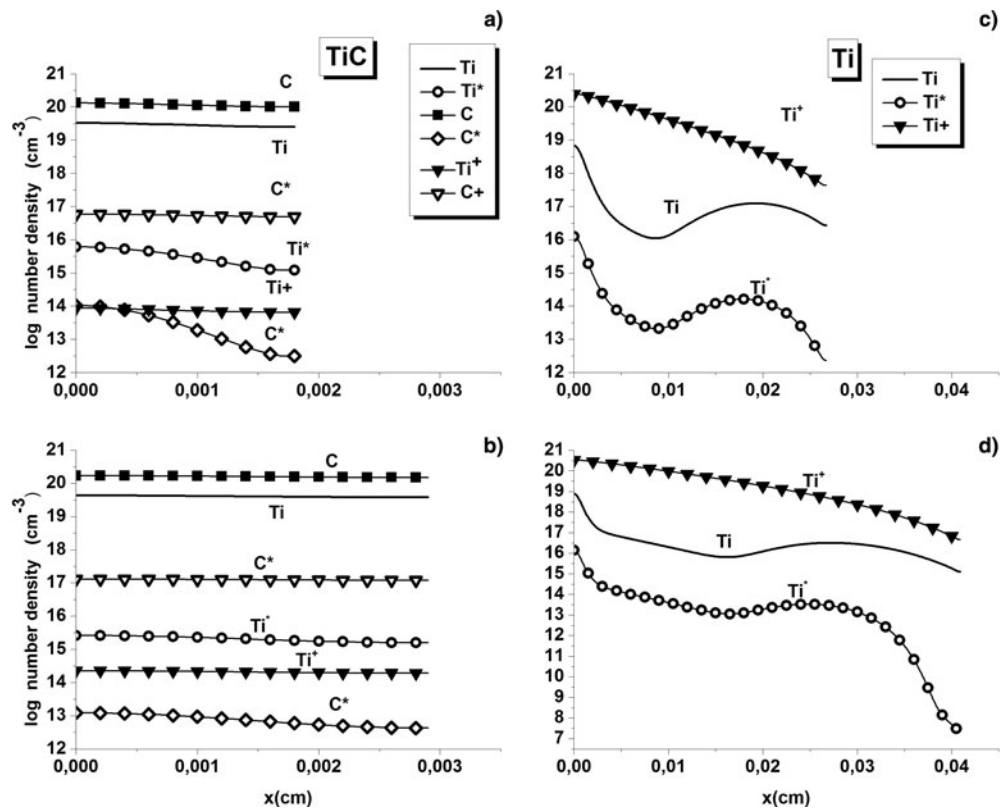


Fig. 13. TiC (a) 12 ns – (c) 18 ns and Ti (b) 12 ns – (d) 18 ns plume species number densities logarithm comparison for the same effective energy.

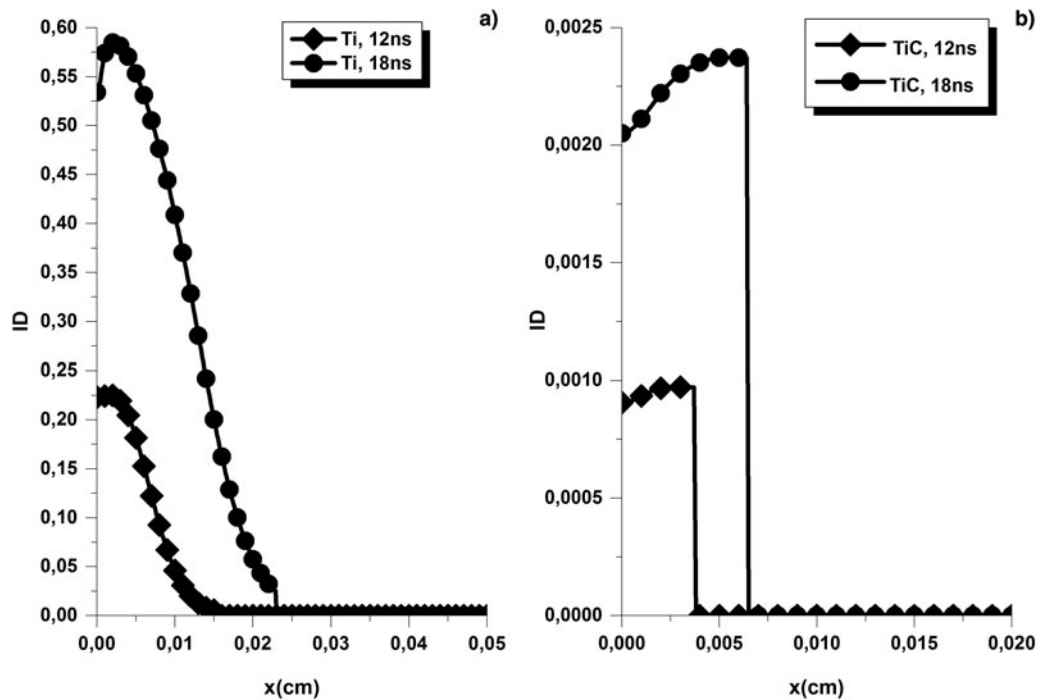


Fig. 14. Ti (a) and TiC (b) plumes ionization degrees for the same ablated mass.

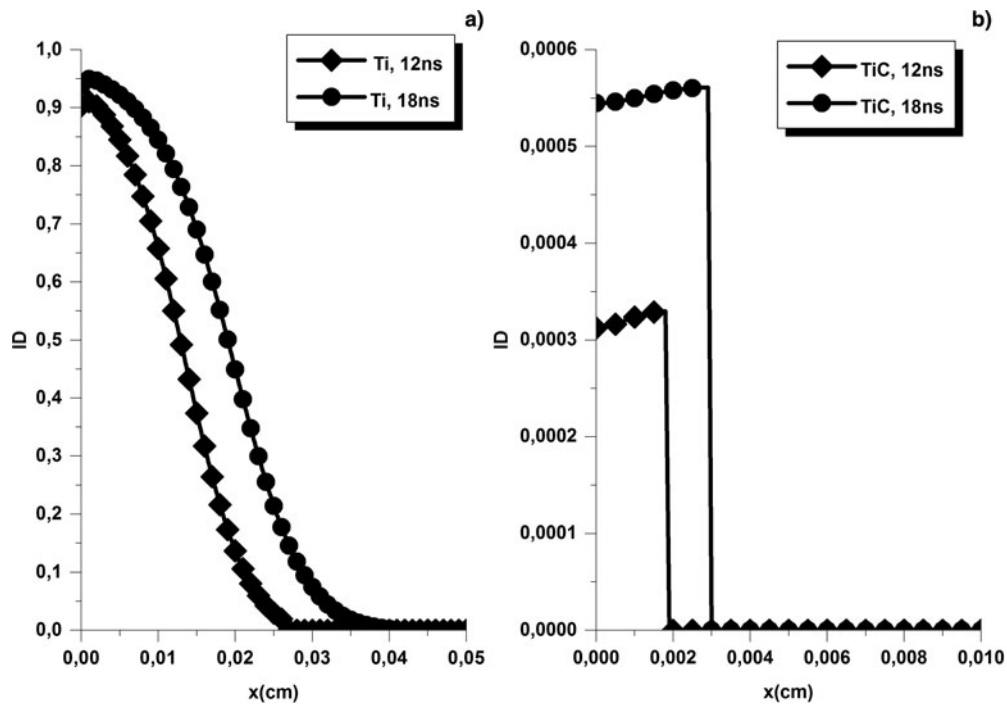


Fig. 15. Ti (a) and TiC (b) plumes ionization degrees for the same effective energy.

both materials receive the same effective energy the plumes with the highest ionization degrees are the ones expanding faster and further.

After examining the above-mentioned results, investigating results for the same amount of plasma shielding (around 32%) also seemed relevant. In this case, the laser beam fluence was  $1.5 \text{ J/cm}^2$  for titanium and  $22 \text{ J/cm}^2$  for TiC.

The examination of the velocities (Fig. 16) of TiC (a) and pure titanium (b) plumes revealed an utterly different behavior of what we investigated until now. Not only the plume velocities are comparable in this case, but it is the TiC plume that is characterized by the highest expansion velocities. The distances to which the plumes expand are also comparable, but titanium plumes are still the ones expanding the furthest from the target surface (in

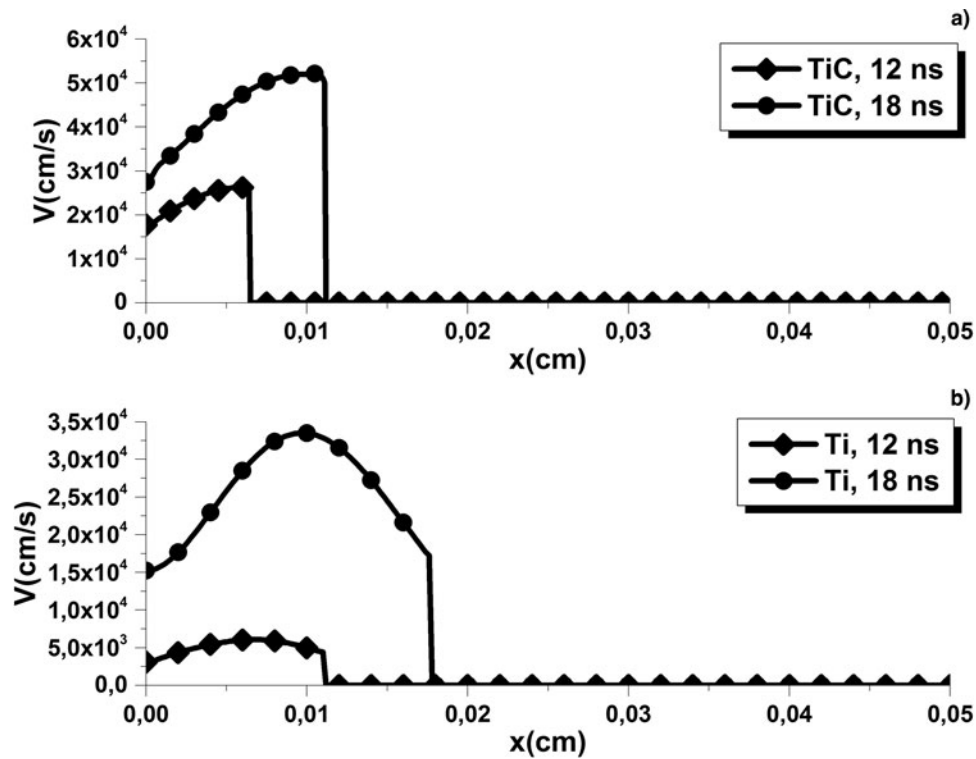


Fig. 16. Ti and TiC plumes velocities for the same plasma shielding rate.

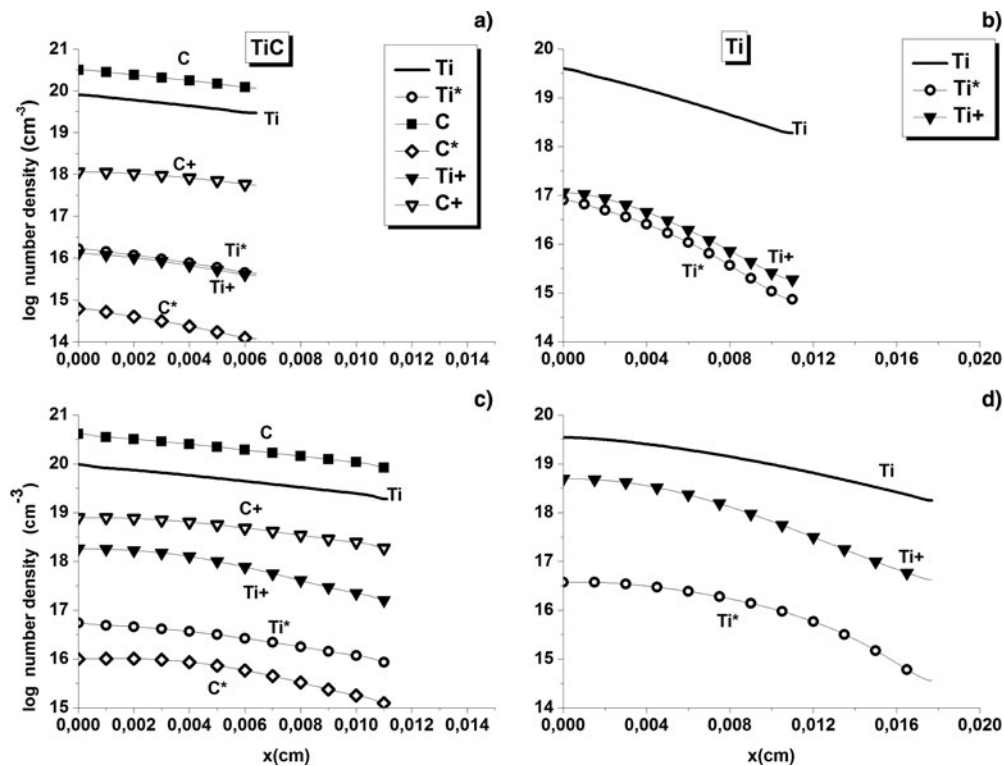


Fig. 17. TiC and Ti plume species number densities logarithm comparison for the same plasma shielding rate.

all the previous cases they were at least ten times longer for titanium plumes). In contrast to all the previously examined cases, under those conditions more mass is ablated from the TiC material:  $1.05 \cdot 10^{-6}$  g against  $5.32 \cdot 10^{-7}$  g. Those results show that to have a faster TiC-induced plume, not only more matter need to

be extracted from the target, but also more energy need to be deposited into the plumes.

Figure 17 shows that even though the TiC is the fastest in those conditions, it is still characterized by high neutral number densities with a dominance of carbon atoms which are characterized by

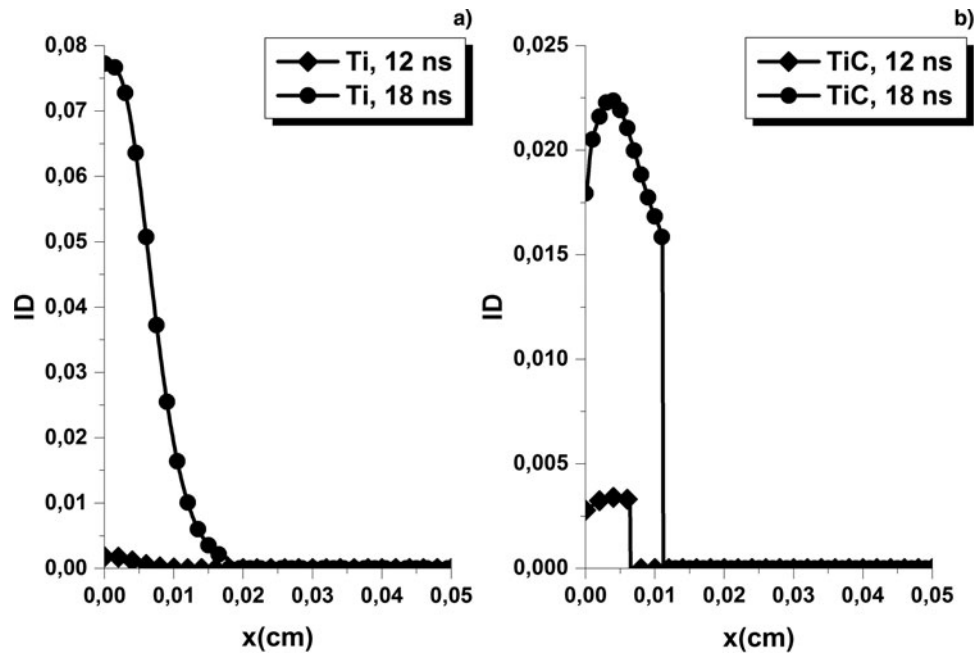


Fig. 18. TiC and Ti plumes ionization degrees for the same plasma shielding rate.

a higher ionization energy level. One can also see that in this case titanium plumes also contain more neutral species and at identical times less ionized titanium than either carbon or titanium in the TiC plasmas.

The results presented in Figure 18 show clearly that the plumes fastest expansions are not necessarily linked to the highest ionization degree.


### Summary conclusion and perspectives

This work was focused on investigating the dynamics of LIP from a ceramic material. A recently developed model was used for that purpose. TiC was chosen for this study. A comparison with the characteristics and dynamics of LIP from a pure titanium material was presented. Links between the target material thermophysical/optical properties as well as plasmas elemental characteristics and plume dynamics were established. Comparisons were made:

- Under the same laser ablation conditions
- For the same effective energy
- For the same ablated mass
- For the same plasma shielding rate

The results demonstrate that the plumes dynamics is intertwined with the materials properties and the nature of the plasmas constituents. To have comparable plume dynamics, plasmas need to be induced from greater amount of matter from TiC targets than pure titanium ones. The plumes dynamics is linked to the amount of species they contain but not necessarily to their ionization degree.

Future studies will be dedicated to developing new models for more complex materials with a focus on including additional physical processes depending on the laser-matter interaction conditions. Including, for example, the internal electrical field and its impact on plumes dynamics would be of great interest.

Author ORCIDs.  A. Ait Oumeziane, 0000-0002-9656-6249.

### References

- Ait Oumeziane AK and Parisse J-D (2018) Toward a comprehensive UV laser ablation modeling of multicomponent materials-A non-equilibrium investigation on titanium carbide. *Physics of Plasmas* **25**, 053511.
- Ait Oumeziane AK, Liani B and Parisse J-D (2014) Laser induced plasma on copper target, a non-equilibrium model. *Physics of Plasmas* **21**, 023507.
- Ait Oumeziane AK, Liani B and Parisse J-D (2016a) Laser-induced plasma on a titanium target, a non-equilibrium model. *Plasma Chemistry Plasma Processing* **36**, 711–730.
- Ait Oumeziane AK, Liani B and Parisse J-D (2016b) Non-equilibrium modeling of UV laser induced plasma on a copper target in the presence of  $\text{Cu}^{2+}$ . *Physics of Plasmas* **23**(3), 033502.
- Boris JP, Landsberg AM, Oran ES and Garner JH (1993) LCPFCT a flux corrected transport algorithm for solving generalized continuity equations. *NRL Memorandum Report* **93**, 7192.
- Clarke P, Dyer PE, Key PH and Snelling HV (1999) Plasma ignition thresholds in UV laser ablation plumes. *Applied Physics A* **69**(Suppl.), S117–S120.
- D'Alessio I, Salvi AM, Teghil R, Marotta V, Santagata A, Brunetti B, Ferro D and De Maria G (1998) Silicon supported TiC films produced by pulsed laser ablation. *Applied Surface Science* **134**, 53–62.
- Dellasega D, Russo V, Pezzoli A, Conti C, Lecis N, Besozzi E, Beghi M, Bottani CE and Passoni M (2017) Boron films produced by high energy pulsed laser deposition. *Materials and Design* **134**, 35–43.
- Eason R (2007) *Pulsed Laser Deposition of Thin Films: Applications-Led Growth of Functional Materials*. Hoboken, New Jersey: John Wiley.
- Harilal SS, O'Shay B, Tao Y and Tillack MS (2006) Ambient gas effects on the dynamics of laser-produced tin plume. *Journal of Applied Physics* **99**, 083303.
- Koral C, Dell'Aglio M, Gaudiuso R, Alrifai R, Torellis M and De Giacomo A (2018) Nanoparticle-enhanced laser induced breakdown spectroscopy for the noninvasive analysis of transparent samples and gemstones. *Talanta* **182**, 253–258.
- Kumar A, Chan HL and Kapat JS (1998) Deposition and characterization of titanium carbide coatings using laser ablation method. *Applied Surface Science* **127–129**, 549–552.
- Lee JH (1985) Basic governing equations for the flight regime of aeroassisted orbital transfer vehicles. *Progress in Astronautics and Aeronautics Thermal Design of Aeroassisted Orbital Transfer Vehicles* **96**, 3–53.

- Mazhukin VI, Nossov VV, Nickiforov MG and Sumorov I** (2003) Optical breakdown on aluminum vapor induced by ultraviolet laser radiation. *Journal of Applied Physics* **93**, 56–66.
- Mendes M and Vilar R** (2003) Influence of the processing parameters on the formation and deposition of particles in UV pulsed laser ablation of  $\text{Al}_2\text{O}_3$ -TiC ceramics. *Applied Surface Science* **217**, 149–162.
- Oliveira V and Vilar R** (2007) Finite element simulation of pulsed laser ablation of titanium carbide. *Applied Surface Science* **253**, 7810–7814.
- Oliveira V, Gomes F and Vilar R** (2005) Column-growth mechanisms during KrF laser micromachining of  $\text{Al}_2\text{O}_3$ -TiC ceramics. *Applied Physics A* **81**, 1157–1162.
- Oran E-S and Boris JP** (1987) *Numerical Simulation of Reactive Flow*. New York: Elsevier.
- Parisse J-D, Sentis M and Zeitoun DE** (2011) Modeling and numerical simulation of laser matter interaction and ablation with 193 nanometer laser for nanosecond pulse. *International Journal of Numerical Methods for Heat and Fluid Flow* **21**, 73–94.
- Ravindra HP** (2005) *Thermal modeling of laser drilling and cutting of engineering materials*, M.S. thesis. Graduate College of the Oklahoma State University.
- Rosen DI, Mitteldorf J, Kothandaraman G, Pirri AN and Pugh ER** (1982) Coupling of pulsed 0.35 micrometer laser radiation to aluminum alloys. *Journal of Applied Physics* **53**, 3190.
- Scharf T and Krebst HU** (2002) Influence of inert gas pressure on deposition rate during pulsed laser deposition. *Applied Physics A* **75**, 551–554.
- Siozos P, Philippidis A and Anglos D** (2017) Portable laser-induced breakdown spectroscopy/diffuse reflectance hybrid spectrometer for analysis of inorganic pigments. *Spectrochimica Acta Part B* **137**, 93–100.
- Stafe M, Marcu A and Puscas N** (2014) *Pulsed Laser Ablation of Solids: Basics, Theory and Applications*. Springer Series in Surface Sciences. Volume 53 Heidelberg, Berlin: Springer-Verlag.
- Strozzi DJ, Bailey DS, Michel P, Divol L, Sepke SM, Kerbel GD, Thomas CA, Ralph JE, Moody JD and Schneider MB** (2017) Interplay of Laser-Plasma Interactions and Inertial Fusion Hydrodynamics PRL 118, 025002.
- Sturm K, Fahler S and Krebs H-U** (2000) Pulsed laser deposition of metals in low pressure inert gas. *Applied Surface Science* **154**, 462–466.
- Teghil R, D'Alessio L, Zaccagnino M, Ferro D, Marotta V and De Maria G** (2001) TiC and TaC deposition by pulsed laser ablation: a comparative approach. *Applied Surface Science* **173**, 233–241.
- Teghil R, D'Alessio L, De Bonis A, Galasso A, Villani P and Santagata A** (2006) Femtosecond pulsed laser ablation and deposition of titanium carbide. *Thin Solid Films* **515**, 1411–1418.
- Thomann AL, Boulmer-Leborgne C and Dubreuil B** (1997) A contribution to the understanding of the plasma ignition mechanism above a metal target under UV laser irradiation. *Plasma Sources Science and Technology* **6**, 298–306.
- Van Driel H** (1986) Kinetics of high density plasmas generated in Si by 1.06 and 0.53 micrometer picosecond laser pulses. *Physical Review B* **35**, 8166.
- Vasantgadkar NA, Bhandarkar UV and Joshi SS** (2010) A finite element model to predict the ablation depth in pulsed laser ablation. *Thin Solid Films* **519**, 1421–1430.
- Williams WS** (1999) Electrical properties of hard materials. *International Journal of Refractory Metals & Hard Materials*. **17**, 21–26.
- Yu H., Li H., Wang Y., Cui L., Liu S and Yang J** (2018) Brief review on pulse laser propulsion. *Optics and Laser Technology* **100**, 57–74.
- Zel'dovitch YB and Raizer YP** (1966) *Physics of Shock Waves and High Temperature Hydrodynamics Phenomena*. New York: Academic Press.